Japanese Journal of Applied Physics

The Japan Society of Applied Physics

REGULAR PAPER

Measurement of viscoelasticity of anisotropic viscoelastic phantom by dual ultrasound excitation

Japanese Journal of Applied Physics **59**, SKKE24 (2020) **REGULAR PAPER**
https://doi.org/**10.35848/1347-4065/ab8bc0**

Measurement of viscoelasticity of anisotropic viscoelastic phantom by dual ultrasound excitation

Hibiki Kawamura[1], Shohei Mori[1], Mototaka Arakawa[1,2*], and Hiroshi Kanai[1,2]

[1]*Graduate School of Engineering, Tohoku University, Sendai 980-8579, Japan*
[2]*Graduate School of Biomedical Engineering, Tohoku University, Sendai 980-8579, Japan*

*E-mail: arakawa@ecei.tohoku.ac.jp

Received December 4, 2019; revised March 20, 2020; accepted April 21, 2020; published online May 22, 2020

An estimation of anisotropic viscoelasticity is important for evaluating muscle lesions. In the previous study, we proposed a method for estimating viscoelasticity in a local region by exciting a phantom specimen from both directions. In the present study, we observed the acoustic field having the locality and directivity generated by dual ultrasound excitation. In addition, the displacement distributions for the isotropic and anisotropic viscoelastic phantoms were measured, and the local generation of large displacement and its directionality was confirmed around the excitation focal point. Furthermore, we applied our viscoelasticity estimation method to the anisotropic viscoelastic phantom. The estimated shear modulus differed depending on the angle between the opposite direction of the ultrasound transducer projected on the phantom surface and longitudinal direction of the cylindrical urethane rubber bundle in the anisotropic viscoelastic phantom. Therefore, the viscoelasticity estimation method in the present study could estimate anisotropic viscoelasticity locally.

1. Introduction

Muscle tissue is composed of bundles of elongated cells called muscle fibers with a diameter of 10–100 μm, so it exhibits anisotropic viscoelastic properties.[1–6)] For example, when shear wave elastography is applied to the brachial muscle, the shear modulus estimated from the velocity of the shear wave propagating parallel to the muscle fiber direction was approximately 4 times larger than that estimated from the velocity of shear wave propagating perpendicular to the muscle fiber direction.[6)] The viscoelastic and anisotropic properties of muscle are closely related to the progression of lesions. For example, the stiffness of the target tissue increased as the disease progressed in Duchenne muscular dystrophy.[7)] In addition, muscle fiber fragmentation due to necrosis caused a decrease in anisotropy.[8)] Muscle tissue became soft as an indication of decreased muscle tone in the case of peripheral neuropathy and pyramidal tract disorders.[9,10)] Athletes' enlarged muscles and contracted muscles were observed as increased stiffness.[9)] Diabetic Pompe type showed an abnormal increase in muscle stiffness and volume.[9)] In amyloidosis, there were cases of increased stiffness and atrophy in muscle.[9)] Therefore, the evaluation of the anisotropic viscoelastic properties of muscle has attracted great clinical interests for the purpose of the diagnoses of muscular diseases and the planning for accurate treatment.[11)] Conventional diagnostic methods for muscle tissues are computed tomography, magnetic resonance imaging, and dual-energy X-ray absorptiometry. However, there are drawbacks such as invasiveness, financial burden, and inability to carry the equipment.[12)] Therefore, ultrasound imaging is considered as a reliable alternative as a non-invasive, low-cost, and portable method.[6)]

When the ultrasound elastography provided as a function of the ultrasound diagnostic apparatus was applied to muscles, the stiffness distribution of muscle tissue was acquired.[13,14)] However, since this is qualitative, it is necessary to estimate viscoelastic parameters quantitatively in order to accurately evaluate the progression of the lesion. The shear wave elastography is used as a quantitative estimation method for elastic properties.[6,7,15–17)] This method can estimate the shear modulus, from the shear velocity and the tissue density. Furthermore, it is possible to estimate the anisotropic viscoelasticity of anisotropic elastic tissues by combining shear wave elastography with shear wave spectroscopy[18)] and rheological models.[6,17)] The acoustic radiation force impulse (ARFI) imaging evaluates the elastic properties from the magnitude of the displacement response by exciting the tissue using pulse wave.[19–24)] It has been studied to estimate the anisotropic viscoelasticity of muscle tissue.[20–24)] However, in order to generate a measurable displacement by several ultrasonic pulses, high-intensity pulsed ultrasound at 1000 W cm^{-2} was required.[19)] According to the safety guideline for the use of diagnostic ultrasound, it is recommended that the intensity of the spatial peak-temporal average is below 240 mW cm^{-2} for pulsed waves and the intensity is less than 1 W cm^{-2} for continuous waves.[25)] The intensity of the pulsed ultrasound employed in the ARFI imaging was therefore far greater than that indicated by the safety guidelines. Anisotropic viscoelasticity was estimated in the recent study, however, the intensity of the pulsed ultrasound was unclear.[20)]

We developed a method to locally excite a tissue by applying dual AM acoustic radiation force.[26,27)] The direction of the main displacement to be generated can be fixed to one axis. In addition, the frequency characteristics of the acoustic radiation force and the displacement on the phantom specimens were measured. Therefore, the relationship of the stress–strain transfer function was obtained indirectly. The viscoelastic parameters of the phantom specimens were estimated by fitting a rheological model to the relationship.[28)] This method could estimate viscoelasticity locally and quantitatively. However, it is necessary to investigate the possibility of estimating anisotropic viscoelasticity to apply this method to the evaluation of muscle.

The purpose of this study is to investigate whether the viscoelastic property estimation method adopted could locally estimate anisotropic viscoelasticity. In our previous study, we investigated the acoustic field formed by the ultrasound excitation.[29)] Furthermore, we investigated the displacement distribution on an isotropic viscoelastic phantom surface generated by ultrasound excitation.[29)] In

the present paper, we investigated the displacement distribution on an anisotropic viscoelastic phantom surface generated by dual ultrasound excitation. Furthermore, we showed that anisotropic viscoelasticity could be estimated.

2. Principle and experimental methods

2.1. Acoustic radiation pressure generated on the tissue surface

Acoustic radiation pressure is generated when a traveling ultrasound wave has an energy difference due to a reflector or an absorber.[30] In the present study, the acoustic radiation pressure was given by applying a sinusoidal signal with two frequency components, f_0 and $(f_0 + \Delta f)$ to two ultrasound transducers with the same specification. Thus, two identical acoustic radiation pressures were generated. When a plane wave with frequency components f_0 and $(f_0 + \Delta f)$ is incident at the angle of incidence θ_i on the tissue along the path, the amplitude of the generated acoustic radiation pressure $P_R(t)$ changes with the frequency Δf as shown in Eq. (1).

$$P_R(t) \approx \frac{2\rho_1 p_1^2 \cos\theta_i}{(\rho_1 c_1 \cos\theta_t + \rho_2 c_2 \cos\theta_i)^2} \times \left[\frac{\rho_2^2 c_2^2}{\rho_1^2 c_1^2}\cos^2\theta_i + \left(1 - 2\frac{\rho_2}{\rho_1}\right)\cos^2\theta_t\right] \times [1 + \cos(2\pi\Delta f t)], \quad (1)$$

where, p_1 is the sound pressure amplitude of the ultrasound just before the incidence, ρ_1 and c_1 are the density and sound velocity of the medium before the incidence, and ρ_2 and c_2 are the density and sound velocity of the medium after the incidence, respectively. θ_t is the angle of refraction.

2.2. Generation of shear strain by dual ultrasound excitation and the influence of anisotropy

Figure 1 shows a schematic diagram of the acoustic radiation force generated in a medium by dual ultrasound excitation. As shown in Fig. 1(a), the focal points of two point-focused ultrasounds coincide and the ultrasounds are irradiated diagonally to the medium surface. When acoustic radiation forces are applied diagonally from both sides, the x-axis direction components of the acoustic radiation forces cancel out each other in the excitation area, so the acoustic radiation force is applied to the medium surface only along the z-axis direction. The magnitude of the z-axis direction component of the acoustic radiation force applied to the medium decreases as the distance from the focal point increases because the focused ultrasounds are irradiated. Figure 2(a) shows a schematic diagram of the distribution of the z-axis direction component of the acoustic radiation force generated by the dual ultrasound excitation, taking up the y–z plane. Focusing on the local area surrounded by the red dotted line in Fig. 2(a), since the magnitude of the z-axis direction component of the acoustic radiation force applied to two adjacent points is different, the difference of the acoustic radiation force is considered to be the shear force in z-axis direction applied to the y–z plane as shown in Fig. 2(b).

In addition, the propagation path length of each excitation ultrasound coincides at the point apart from the focal point in the y-axis direction, however, it differs at point apart from the excitation focal point in the x-axis direction as shown in Fig. 3. The phase difference occurs between two excitation ultrasounds along the x-axis direction on the medium surface. Due to the effect of this phase difference, the magnitude of the z-axis component of the acoustic radiation force on the x–z plane variates periodically as it moves away from the focal point in the x-axis direction as shown by the blue line in Fig. 4. When the speed of sound in water is 1500 m s^{-1}, the frequency of the excitation ultrasound is 1 MHz, and the incidence angle of the excitation ultrasound on the object surface is 35°, the magnitude of the acoustic radiation force exhibits maxima and minima every 0.92 mm away from the focal point in the x-axis direction. Therefore, it is considered that the z-axis component of the acoustic radiation force decreases greatly when moving away from the focal point in the x–z plane compared to the y–z plane as shown in Fig. 4. Then, it is considered that the generated shear force in the z-axis direction increases because the difference between the forces in the z-axis direction of the two adjacent points is larger in the x–z plane. Therefore, the magnitude of shear

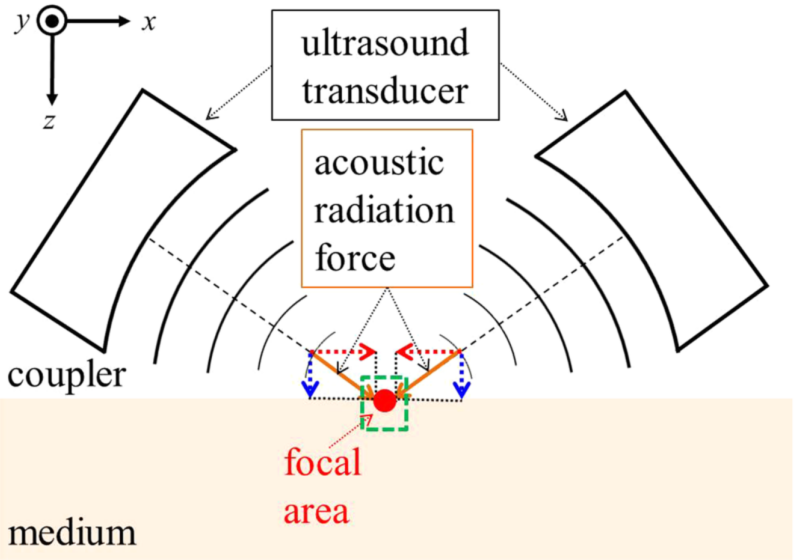

Fig. 1. (Color online) Schematic diagram of the acoustic radiation force generated by dual ultrasound excitation.

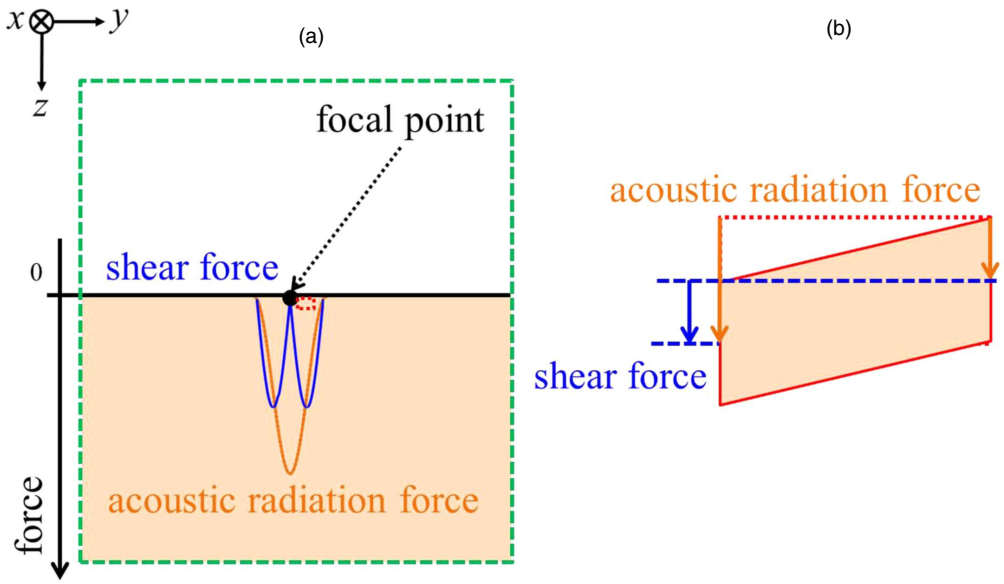

Fig. 2. (Color online) (a) Schematic diagram of the z-axis direction component of acoustic radiation force and the shear force in z-axis direction generated by dual ultrasound excitation. (b) The shear force generated by the difference in the magnitude of the z-axis direction component of acoustic radiation force between two adjacent points in the area surrounded by the red dotted line in (a).

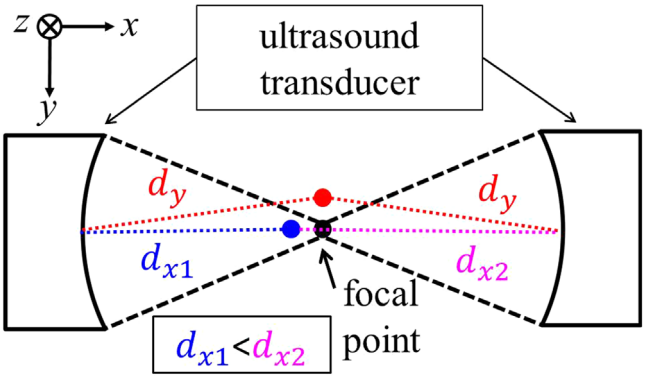

Fig. 3. (Color online) Schematic diagram of the propagation path length of each excitation ultrasound at points equidistant from the focal point in dual ultrasound excitation. d_y: distance from a point away in y-axis direction from the focal point to both ultrasound transducers. d_{x1}: distance from point away in x-axis direction from the focal point to the left ultrasound transducer. d_{x2}: distance from point away in x-axis direction from the focal point to the right ultrasound transducer.

force in the z-axis direction in the x–z plane can be generated larger than that in the y–z plane by dual ultrasound excitation. We consider that dual ultrasound excitation can apply shear force in the z-axis direction having directivity on the medium surface.

Next, we consider the elastic modulus of an anisotropic viscoelastic material having a structure in which elongated fibers are bundled like muscle. It has a large elastic modulus in the axial direction of the fiber bundle due to the strong binding force among tissues. By contrast, the elastic modulus in the radial direction of the fiber bundle is small because the bonding force among fibers is weaker than the bonding force between tissues. Therefore, it is considered that the anisotropy of viscoelasticity is caused by the difference in the bonding force depending on the structure. Figure 5 shows a schematic diagram of the shear strain in the z-axis direction generated when an acoustic radiation force having a distribution of z-axis direction components as shown in Fig. 2(a) is applied to an anisotropic viscoelastic material with a fiber bundle structure. Figures 5(a) and 5(b) show the schematic diagrams when the acoustic radiation force is applied in the axial and the radial directions of the fiber bundle, respectively. Due to the difference in elastic modulus caused by the bonding force depending on the structure, the shear strain in the z-axis direction generated by applying the acoustic

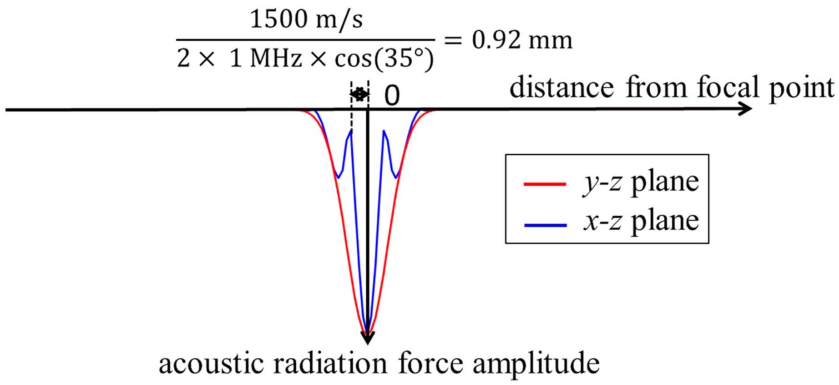

Fig. 4. (Color online) Schematic diagram of the distribution of the z-axis direction component of acoustic radiation force generated on each plane by dual ultrasound excitation. Red line: on the y–z plane, and blue line: on the x–z plane.

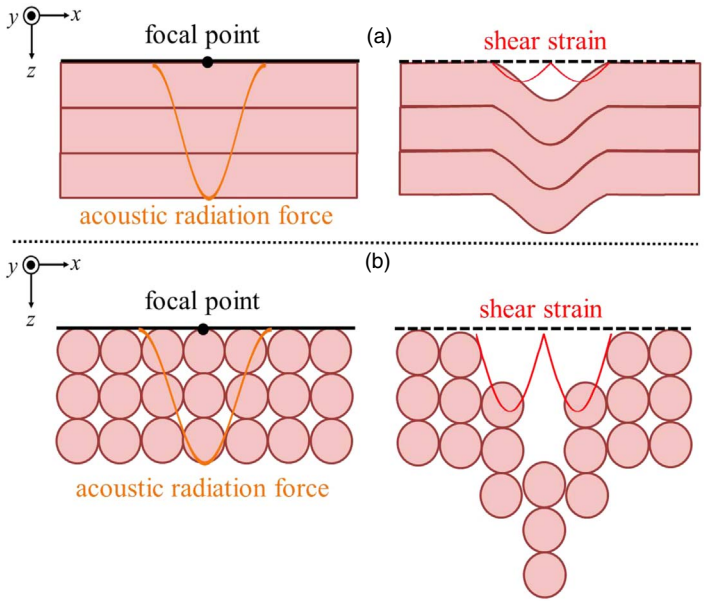

Fig. 5. (Color online) The shear strain in the z-axis direction in an anisotropic viscoelastic body with a fiber bundle generated by applied the acoustic radiation force having the distribution of the z-axis direction component. Directions in which acoustic radiation force is applied are (a) the axial direction of the fiber and (b) the radial direction of the fiber.

radiation force having a distribution of z-axis direction components to the radial direction of the fiber bundle is greater than that by applying it to the axial direction of the fiber bundle. When acoustic radiation force is applied to an anisotropic viscoelastic material with a fiber bundle structure by dual ultrasound excitation, the magnitude of the shear strain in the z-axis direction is mainly related to the angle between the x–z plane and the fiber bundle since the shear force in the z-axis direction generated on the x–z plane is larger than that on the y–z plane. Therefore, since the shear force in the z-axis direction generated by dual ultrasound excitation has directivity, the anisotropy of viscoelasticity of the anisotropic viscoelastic material with a fiber bundle structure could be detected by measuring the shear strain in the z-axis direction.

2.3. Experimental method

Figure 6 shows the experimental arrangement in the present study. Two concave transducers (TR1, TR2) with a center frequency f_0 of 1 MHz, an aperture half-angle of 22.6°, an effective aperture diameter of 50 mm, and a focal length of 60 mm were used for ultrasound excitation. They were opposed with an irradiation angle of 35° to the phantom. The focal points of the two ultrasound transducers coincided with the center of the phantom surface, and this point was treated as the center of distribution measurements of the acoustic field and the displacement. Sinusoidal signals with frequencies of f_0 and $(f_0 + \Delta f)$ generated by a function generator (Tektronix, Inc., AFG2020) were summed up, amplified, and applied to the transducers. The applied voltage to each transducer was 37.5 V. The sound pressure of the continuous ultrasound generated at the focal point by dual ultrasound excitation was 280 kPa, which corresponds to 2.6 W cm^{-2} in ultrasound intensity. This intensity is 2.6 times higher than the recommended intensity in the safety guideline.[25] However, this study is a basic study aimed at establishing a method for estimating anisotropic viscoelasticity, and the intensity does not affect the estimation result. Therefore, this intensity was used for the experiment. For the measurement of the acoustic field, we replaced the phantom with a hydrophone (Toray Industries, Inc., NH8133) as shown in Fig. 6(b). It was installed parallel to the z-axis to measure the z-axis direction component of the sound pressure. The output signal of the hydrophone was input to the FFT analyzer (Ono Sokki Co. Ltd., CF-930), and the frequency spectrum was acquired to extract the excitation frequency Δf component of the sound pressure. The excitation frequency Δf was set as 20 Hz.

The phantom simulating biological soft tissues with a size of $40 \times 40 \times 43$ mm^3 was prepared by Asker-C hardness 7 urethane resin with 2 wt% graphite. In addition, an anisotropic viscoelastic phantom was prepared by bundling 100 cylindrical urethane rubbers with a diameter of 300 μm and hardening them with Asker-C hardness 0 urethane resin. The displacement perpendicular to the phantom surface was measured by the laser displacement meter (Keyence Corp., LK-G80). The measurement range of the laser displacement meter is 75.2 ± 14 mm. The phantom, ultrasound transducers, and laser displacement meter shown in Fig. 6(a) have the same dimension ratio as the experimental arrangement. Only the phantom caused light reflection within the measurable range. Therefore, the displacement of the phantom surface could be measured by the laser displacement meter. The sampling frequency of the laser displacement meter was set to 5000 Hz. The output signal of the laser displacement meter was input to the FFT analyzer to extract the Δf component of the displacement. The excitation frequency Δf was set as 20 Hz.

The viscoelasticity estimation method of our research group[28] was applied to the measured frequency characteristics of the stress–strain relationship for the anisotropic viscoelastic phantom. The direction opposing the ultrasound transducer on the x–y plane was set as $\theta = 0°$. Cylindrical urethane rubber bundles in the phantom were placed at three angles of $\theta = 0°$, 45°, and 90°, and the displacement at each

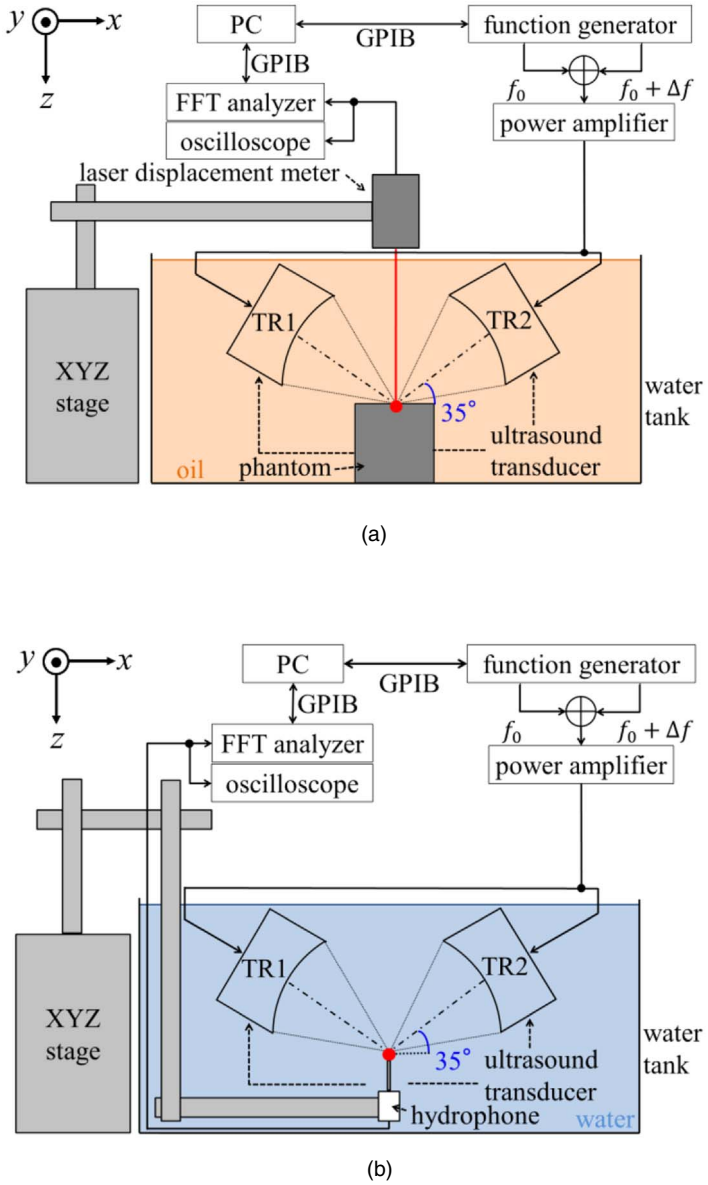

Fig. 6. (Color online) Experimental arrangement employed in the present study. (a) Displacement distribution measurement. (b) Acoustic field measurement.

excitation focal point was measured. The frequency characteristics of the displacement were measured by changing the excitation frequency Δf in the range of 5–2000 Hz. Similarly, the frequency characteristics of acoustic radiation force were measured by exciting an accelerometer (Yamaichi Electronics, 111BW). The relative compliance was calculated from the frequency characteristics of the displacement and the acoustic radiation force. Viscoelastic parameters were estimated by fitting a rheological model to the calculated relative compliance.

3. Results

3.1. Acoustic field

Figure 7 shows the measurement result of the acoustic field by the dual excitation acquired at 0.2 mm intervals. The results were normalized by the maximum sound pressure. The contour lines at −8, −13 and −18 dB were ellipses with the *y*-axis as the major axis. Since these contours are denser in the *x*-axis direction than in the *y*-axis direction, it was clearly confirmed that the sound pressure decreased rapidly in the *x*-axis direction as the distance from the focal point increased. It caused an increase of the difference between the forces at two adjacent points and the generated shear force in the *z*-axis direction in the *x*-axis direction. Therefore, a large shear force in the *z*-axis direction could be generated in the *x*-axis direction in dual ultrasound excitation. The area within the 3 dB contour line in Fig. 7 was 0.8 mm^2, so it was also confirmed that sound pressures were locally applied. Therefore, the local acoustic field was observed near the excitation focal point.

3.2. Displacement distribution in the isotropic viscoelastic phantom

Figure 8 shows the measurement result of the displacement distribution on the isotropic viscoelastic phantom by the dual excitation acquired at 0.2 mm intervals. The elliptical contour lines with the major axis in the *y*-axis direction were confirmed similar to Fig. 7. Since these contours are dense in the *x*-axis direction, it was considered that a large shear strain in the *z*-axis direction was generated in the *x*-axis direction. Therefore, the displacement distribution generated by dual excitation was affected by the directivity of the acoustic field. However, compared to the measurement result

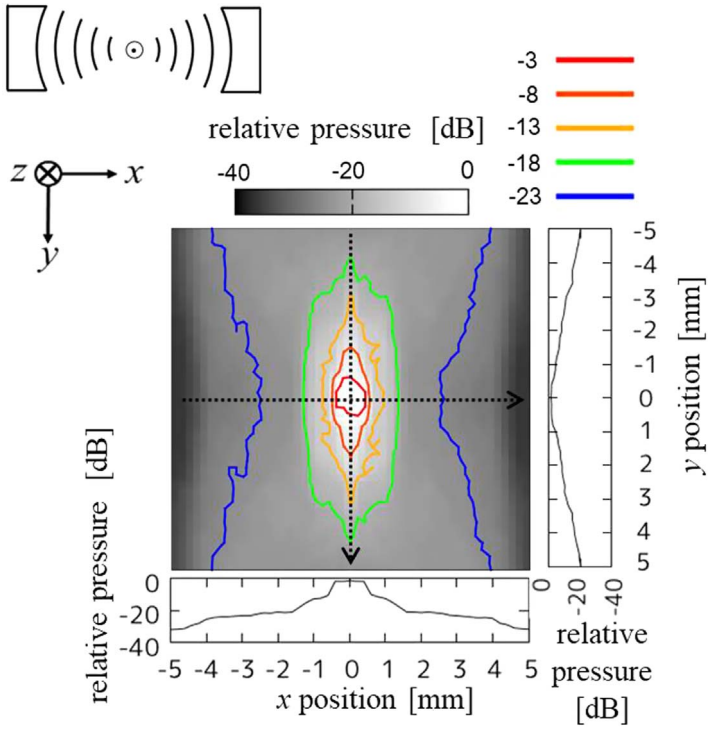

Fig. 7. (Color online) The measurement result of the acoustic field generated by dual ultrasound excitation. Measurement range: 10×10 mm^2, measurement interval: 0.2 mm.

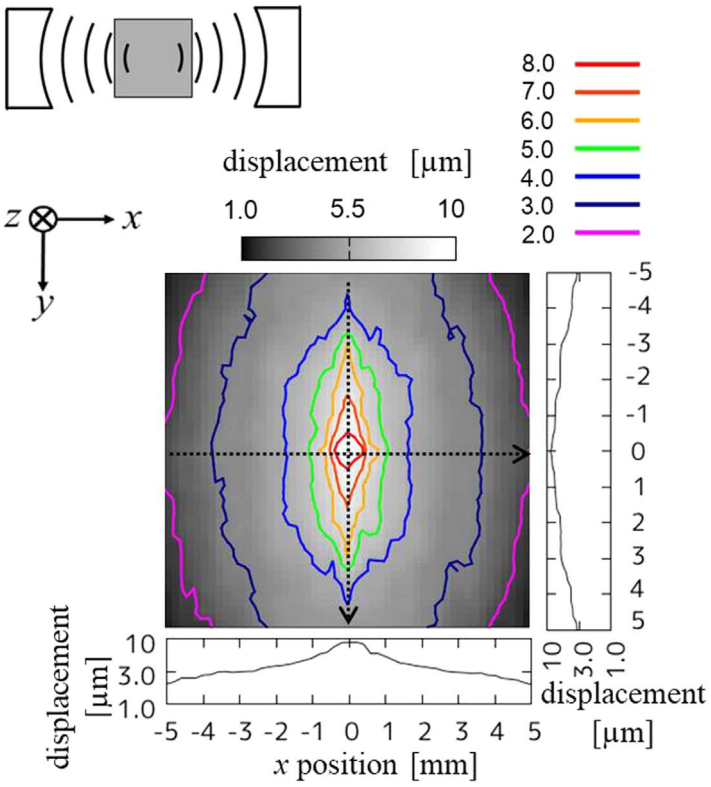

Fig. 8. (Color online) The measurement result of displacement distribution on the isotropic viscoelastic phantom generated by dual ultrasound excitation. Measurement range: 10×10 mm^2, measurement interval: 0.2 mm.

of the acoustic field, the displacement measurement result confirmed that the decrease in displacement amplitude when moving away from the focal point in the x-axis direction was gentler. However, the area within the 7 μm contour line in Fig. 8 was 2.8 mm^2, so it was confirmed that the displacement generated by dual excitation was local.

3.3. Displacement distribution in the anisotropic viscoelastic phantom

Figures 9(a) and 9(b) show the displacement distribution on anisotropic viscoelastic phantom by the dual excitation. They were measured at 0.5 mm intervals. The directions of the cylindrical urethane rubber bundle in the phantom were

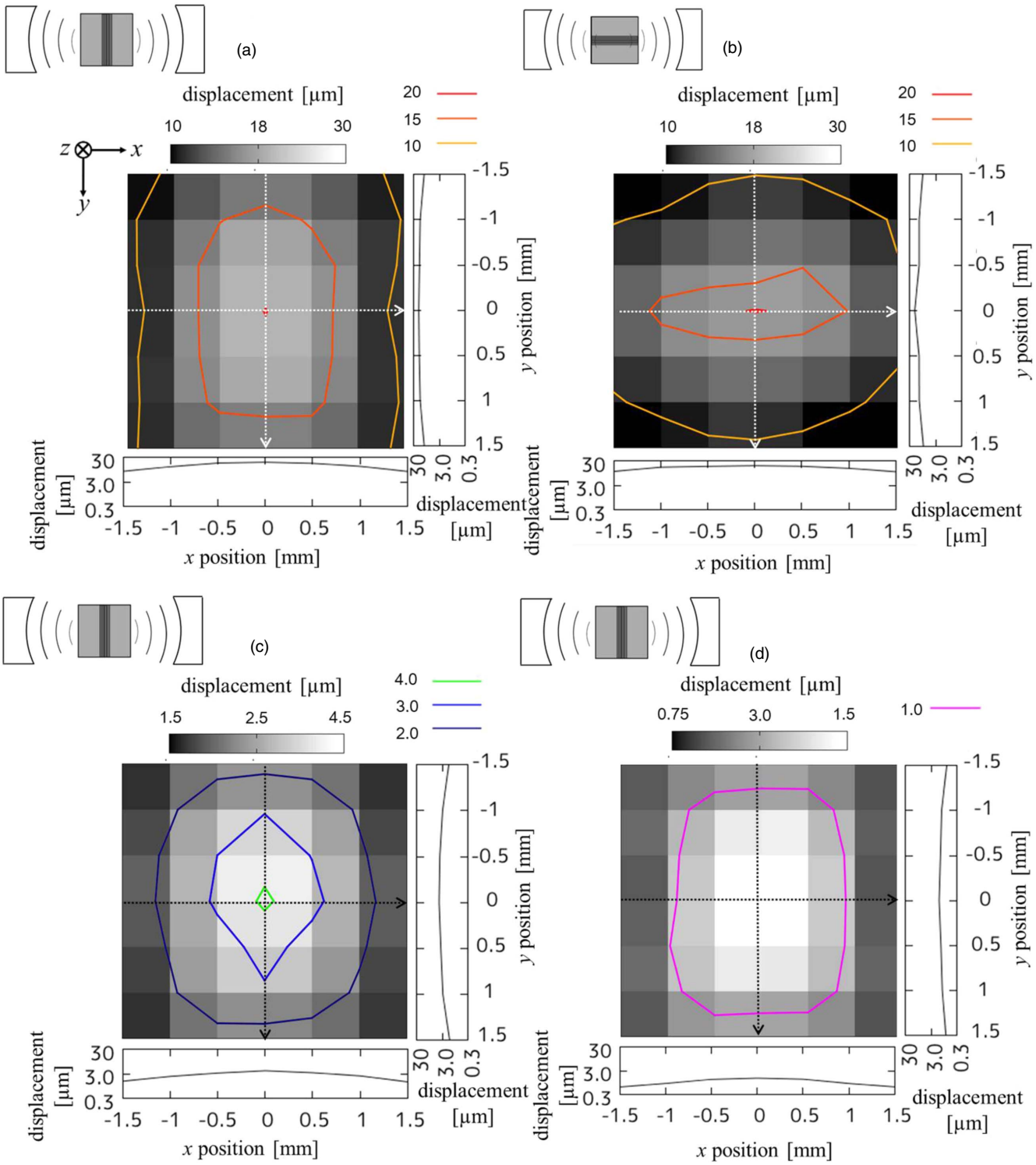

Fig. 9. (Color online) Displacement distribution on the anisotropic viscoelastic phantom generated by dual ultrasound excitation. (a) $\Delta f = 20$ Hz, fiber direction: parallel to y-axis. (b) $\Delta f = 20$ Hz, fiber direction: parallel to x-axis. (c) $\Delta f = 55$ Hz, fiber direction: parallel to y-axis. (d) $\Delta f = 200$ Hz, fiber direction: parallel to y-axis.

installed parallel and perpendicular to the y-axis in Figs. 9(a) and 9(b), respectively. Compared with Fig. 8, the contour lines spread in the x-axis direction in Fig. 9(b) although there was no significant change in Fig. 9(a).

Furthermore, Figs. 9(c) and 9(d) are measurement results under the same conditions as Fig. 9(a) except for Δf. Δf were set as 55 Hz and 200 Hz in Figs. 9(c) and 9(d), respectively. In both Figs. 9(c) and 9(d), displacement distributions similar to that in Fig. 9(a) were measured. Therefore, there was almost no difference in the displacement distribution measured by changing the excitation frequency Δf.

3.4. Estimation of viscoelasticity of anisotropic viscoelastic phantom

Figure 10 shows the calculated relative compliance for $\theta = 0°$, 45°, and 90°. According to the results shown in Fig. 10, the relative compliance did not depend on frequency when low-frequency stress was applied. Its behavior followed

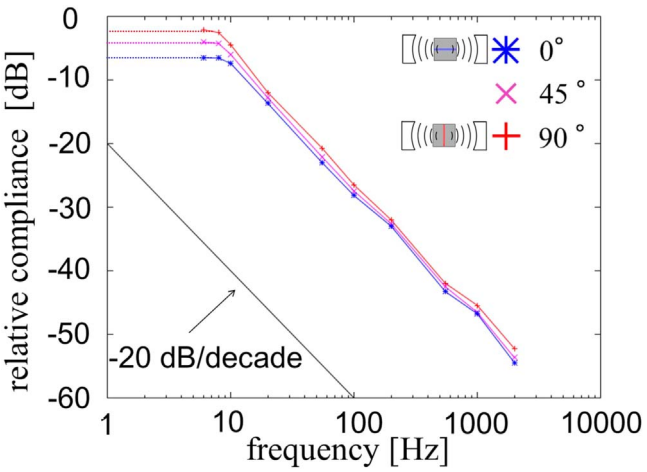

Fig. 10. (Color online) Relative compliance on the anisotropic viscoelastic phantom. Blue line: $\theta = 0°$, purple line: $\theta = 45°$, and red line: $\theta = 90°$.

the frequency characteristics of the Voigt model which is a typical viscoelastic model. Therefore, inflection point G/η and relative shear modulus G were estimated by fitting the frequency characteristics of the Voigt model. The estimated inflection points G/η were 8 Hz at $\theta = 0°$, 6 Hz at $\theta = 45°$, and 5 Hz at $\theta = 90°$. Furthermore, assuming that G estimated from the relative compliance values at the low-frequency region where they became constant was 1 at 90°, they were 1.2 and 1.6 at 45° and 0°, respectively. When viscosity η was estimated from the estimated G/η and G, η was estimated to be almost constant. It is considered that η hardly changes by changing the direction of the cylindrical urethane rubber bundle of the phantom. Therefore, the estimated shear modulus for the direction of the cylindrical urethane rubber bundle parallel to the opposing direction of the excitation ultrasound was explicitly larger than that for the perpendicular direction.

4. Discussion

At first, we discuss the factor that the directivities of the displacement distribution in Fig. 8 were smaller than those of the acoustic field in Fig. 7. Since the phantom was elastically continuous, by locally applying the strong acoustic radiation force, displacements of frequency Δf were generated not only at the applied point but also around it caused by the propagation of the shear wave. Therefore, the measured displacement distribution became the sum of the shear displacement directly generated by the acoustic radiation force and the displacement indirectly caused by the propagation of shear waves generated by the large acoustic radiation force near the focal point. The propagation attenuation of shear waves depends on the frequency, and it was 1.1 dB mm^{-1} when Δf was 20 Hz.[28] The decrease of the displacement of the shear wave at a point 5 mm away from the focal point in the x-axis direction was estimated as 6 dB. In Fig. 7, the sound pressure at that point was more than 20 dB lower than the sound pressure at the focal point. Therefore, we considered that the shear wave generated by a large acoustic radiation force near the focal point had a greater influence indirectly on the measurement of displacement than the shear displacement generated directly by the small acoustic radiation force. As a result, it is considered that the directivity of the displacement distribution was smaller than the directivity of the acoustic field.

Next, we consider the reason that the contour lines of the displacement distribution in Fig. 9(b) spread in the direction of the cylindrical urethane rubber bundle of the phantom compared to that in Fig. 8. Figures 11(a) and 11(b) show the displacement distributions on the x-axis and y-axis of Figs. 8 and 9(b), respectively. The black and red lines show the displacement distribution of the isotropic (Fig. 8) and anisotropic [Fig. 9(b)] phantoms, respectively. Each displacement distribution in the range of ±1.5 mm was shown. In Fig. 11(a), the differences in displacement for each phantom were 11 and 13 μm at the focal point and −1 mm, respectively. The displacement distribution of the isotropic phantom was affected by the directivity of the acoustic field. Since the acoustic field generated by dual ultrasound excitation decreased rapidly in the x-axis direction, the generated displacement on the isotropic phantom decreased as the distance from the excitation focus increased. In contrast, since the direction of the cylindrical urethane rubber bundle was parallel to the measurement direction, it is considered that the propagation of shear wave generated near the focal point along the cylindrical urethane rubber bundle was observed. Therefore, the displacement measured on the anisotropic phantom has a large amplitude even when it was away from the focal point. In Fig. 11(b), the displacement differences for each phantom were 11 and 6 μm at the focal point and −1 mm, respectively. Since the acoustic field generated by dual ultrasound excitation decreased gently in the y-axis direction, the generated displacement on the isotropic phantom was almost unchanged as the distance from the excitation focus increased. In contrast, since the direction of the cylindrical urethane rubber bundle was perpendicular to the measurement direction, it is considered that the amplitude of the shear wave attenuated every time as it crossed the cylindrical urethane rubber caused by the difference of acoustic impedances between urethane rubber and urethane

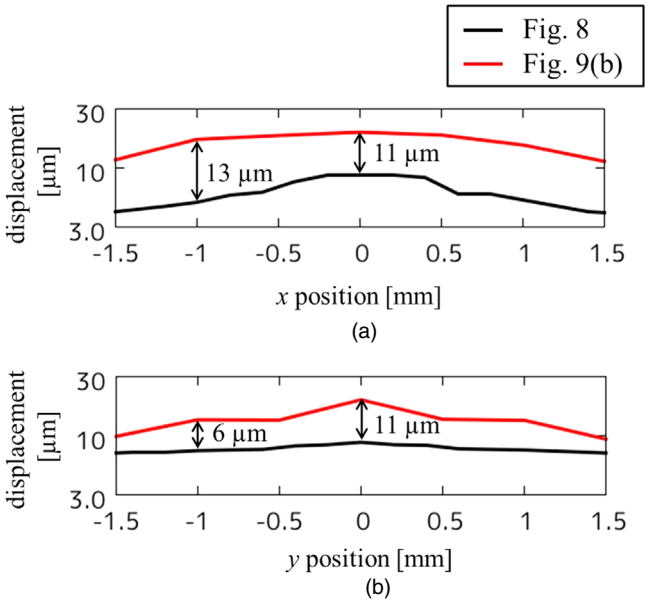

Fig. 11. (Color online) Displacement distributions on the isotropic phantom (Fig. 8) and the anisotropic phantom [Fig. 9(b)] with a fiber direction parallel to x-axis. (a) On x-axis. (b) On y-axis. Black lines: isotropic phantom, and red lines: anisotropic phantom.

resin. Therefore, the displacement measured with the anisotropic phantom decreased as the distance from the excitation focus increased. At the point where the acoustic radiation force was significantly smaller than the focal point, considering that the propagation of shear wave had a larger influence on the displacement measurement than the shear displacement generated directly by the acoustic radiation force, it is considered that the contour lines spread in the longitudinal direction of the cylindrical urethane rubber bundle due to the propagation of the shear wave along the cylindrical urethane rubber bundle rather than the directivity of the acoustic field.

The relative shear modulus was greater when the direction of the cylindrical urethane rubber bundle in the phantom was placed parallel to the opposite direction of the ultrasound transducer on the x–y plane than when it was placed perpendicular to that direction in Fig. 10. This result indicates that the shear modulus in the axial direction of the urethane rubber bundle was larger than the shear modulus in the radial direction since the shear force in the z-axis direction generated on the x–z plane is larger than that on the y–z plane. Similar results were obtained by other measurement methods.[6,17,20] Therefore, it is considered that our method was also able to obtain anisotropic viscoelasticity. In addition, from the results in Figs. 6(a), 6(c) and 6(d), the tendency of the displacement distribution does not greatly depend on the excitation frequency Δf. Therefore, our method has the possibility to evaluate the two-dimensional distribution of anisotropic viscoelasticity.

In the phantom experiment, it is considered that the displacement related to compressive strain was measured in addition to the displacement related to shear strain since the displacement of the phantom surface was measured. Therefore, the estimated anisotropic viscoelasticity might include the effect of displacement related to compressive strain. Considering that the shear modulus and the compressive modulus are proportional to the square of the sound velocity of the shear wave and longitudinal wave in the phantom, respectively, the compressive modulus is much larger than the shear modulus since the velocity of longitudinal waves (approximately $1500\,\mathrm{m\,s^{-1}}$) is much faster than that of shear waves (approximately $10\,\mathrm{m\,s^{-1}}$). Therefore, the displacement related to the compressive strain generated by dual ultrasound excitation is small and negligible for the displacement related to the shear strain. Therefore, we considered that the viscoelasticity was estimated based on the assumption that the measured displacement was mainly related to shear strain. Furthermore, since the displacement on the phantom surface was measured, it is difficult to discuss the events occurring inside the fiber bundle structure. It is unclear how much the effects of reflection and refraction at the boundaries inside the fiber bundle structure affect the estimation results. In the future, we discuss this effect by measuring the displacement inside the fiber structure using ultrasonic waves.

5. Conclusions

We measured the acoustic field generated by dual ultrasound excitation. The formed acoustic field in dual ultrasound excitation had directivity in the direction perpendicular to the opposing direction of the transducer and the excitation region was local. We measured the displacement distribution generated by dual ultrasound excitation for an isotropic viscoelastic phantom. The displacement distribution was directional in the same direction as directivity of the acoustic field, however, the influence of the directivity of the acoustic field was small at the point where the sound pressure was small. We considered that this was indirectly caused by the propagation of shear waves generated by a large sound pressure near the focal point has a greater influence on the measurement at the point where the sound pressure was small. We also measured the displacement distribution for an anisotropic viscoelastic phantom. In the anisotropic phantom, the contour lines of the displacement distribution spread in the direction of the cylindrical urethane rubber bundle compared with the result for the isotropic phantom. We considered that this result was caused by the effects of the propagation of shear waves along the direction of the cylindrical urethane rubber bundle rather than the directivity of the acoustic field. We applied the viscoelasticity estimation method of our research group to the anisotropic viscoelastic phantom. The estimated shear modulus differed depending on the angle between the direction that shear force generated by dual ultrasound excitation is large and the longitudinal direction of the cylindrical urethane rubber bundle. This was similar to the literature.[6,17,20] Therefore, our viscoelasticity estimation method can be applied to the evaluation of anisotropy of the anisotropic viscoelastic tissues. Considering that the tendency of the displacement distribution did not change with the excitation frequency, the method of our research group may be able to evaluate the two-dimensional distribution of anisotropic viscoelasticity.

In the future, we plan to examine the applicability of biological tissues by estimating anisotropic viscoelasticity such as chicken breast.

Acknowledgments

This work was partially supported by JSPS KAKENHI 19K22943.

1) R. Carola, J. P. Harley, and C. R. Noback, *Human Anatomy & Physiology* (McGraw-Hill, New York, 1992) 2nd ed., p. 251.
2) K. Hoyt, T. Kneezel, B. Castaneda, and K. J. Parker, Phys. Med. Biol. **53**, 4063 (2008).
3) M. W. Urban, S. Chen, and M. Fatemi, Curr. Med. Imaging Rev. **8**, 27 (2012).
4) M. Wang, B. Byram, M. Palmeri, N. Rouze, and K. Nightingale, IEEE Trans. Med. Imaging **32**, 1671 (2013).
5) M. R. Selzo, C. J. Moore, M. M. Hossain, M. L. Palmeri, and C. M. Gallippi, IEEE Trans. Ultrason. Ferroelectr. Freq. Control **63**, 1276 (2016).
6) J. L. Gennisson, T. Deffieux, E. Macé, G. Montaldo, M. Fink, and M. Tanter, Ultrasound Med. Biol. **36**, 789 (2010).
7) L. Lacourpaille, F. Hug, A. Guével, Y. Péréon, A. Magot, J. Y. Hogrel, and A. Nordez, Muscle Nerve **51**, 284 (2015).
8) E. C. Qin, L. Jugé, S. A. Lambert, V. Paradis, R. Sinkus, and L. E. Billston,, Radiology **273**, 726 (2014).
9) S. Shoji, *Kin Shikkan no Shindan to Chiryo* (Nagai Shoten, Osaka, 1988) , p. 27, [in Japanese].
10) S. Sato and T. Inoue, *Byotai Seiri Bijuaru Mappu 4* (Igaku shoin, Tokyo, 2010) , p. 137, [in Japanese].
11) T. Deffieux, J. Gennisson, M. Tanter, and M. Fink, IEEE Trans. Ultrason. Ferroelectr. Freq. Control **55**, 2177 (2008).
12) A. J. Cruz-Jentoft et al., Age Aging **39**, 412 (2010).
13) Ł. Paluch, E. N. Laskus, J. Wieczorek, B. Mruk, M. Frel, and J. Walecki, Pol. J. Radiol. **81**, 240 (2016).
14) E. Drakonaki, G. M. Allen, and D. J. Wilson, Br. J. Radiol. **85**, 1435 (2012).

15) S. F. Eby, P. Song, S. Chen, Q. Chen, J. F. Greenleaf, and K. N. An, J. Biomech. **46**, 2381 (2013).
16) Y. Yamakoshi, M. Yamazaki, Y. Ishimori, and K. Taniuchi, Jpn. J. Appl. Phys. **57**, 07LF19 (2018).
17) S. Aristizabal, C. Amador, B. Qiang, I. Z. Nenadic, J. F. Greenleaf, and M. W. Urban, IEEE IUS, 2014, p. 3.
18) T. Deffieux, G. Montaldo, M. Tanter, and M. Fink, IEEE Trans. Med. Imaging **28**, 313 (2009).
19) K. Nightingale, M. S. Soo, R. Nightingale, and G. Trahey, Ultrasound Med. Biol. **28**, 227 (2002).
20) C. J. Moore, M. M. Hossain, and C. M. Gallippi, 2017 IEEE IUS, 2017.
21) M. M. Hossain and C. M. Gallippi, Med. Imaging: Ultrason. Imaging Tomogr. **10955**, 109550D (2019).
22) D. Hwang, Y. J. Shin, J. Y. Choi, S. J. Jung, and S. Yang, Ultrasound Imaging Med. **9**, 158 (2019).
23) K. Nightingale, R. Nightingale, D. Stutz, and G. Trahey, Ultrason. Imaging **24**, 100 (2002).
24) J. Dastgir et al., Neuromuscular Disorders **23**, 811 (2013).
25) Japan Society of Ultrasonics in Medicine, Cho-Onpa Igaku **11**, 41 (1984), [in Japanese].
26) H. Hasegawa, M. Takahashi, Y. Nishio, and H. Kanai, Jpn. J. Appl. Phys. **45**, 4706 (2006).
27) Y. Odagiri, H. Hasegawa, and H. Kanai, Jpn. J. Appl. Phys. **47**, 4193 (2008).
28) R. Watanabe, M. Arakawa, and H. Kanai, Jpn. J. Appl. Phys. **57**, 07LF09 (2018).
29) H. Kawamura, S. Mori, M. Arakawa, and H. Kanai, Proc. Symp. Ultrason. Electr., 2019 **Vol. 40**, 1P5-14.
30) G. R. Torr, Am. J. Phys. **52**, 402 (1984).